Wiley
Journal of Food Biochemistry
Volume 2025, Article ID 8016598, 17 pages
https://doi.org/10.1155/jfbc/8016598

WILEY

Research Article

Phytochemical Profile and Evaluation of the Antioxidant, Anticancer, and Antimicrobial Potential of *Artocarpus lacucha* Bark Extracts: In Vitro and In Silico Studies

Md. Junaid Haruni, Mst. Shahnaj Parvin, Sirajum Munira, and Md. Ekramul Islam

Department of Pharmacy, University of Rajshahi, Rajshahi 6205, Bangladesh

Correspondence should be addressed to Mst. Shahnaj Parvin; shahnaj_parvin@ru.ac.bd and Md. Ekramul Islam; ekram@ru.ac.bd

Received 2 April 2025; Revised 26 May 2025; Accepted 31 May 2025

Academic Editor: Marcos Dos Santos Lima

Copyright © 2025 Md. Junaid Haruni et al. Journal of Food Biochemistry published by John Wiley & Sons Ltd. This is an open access article under the terms of the Creative Commons Attribution License, which permits use, distribution and reproduction in any medium, provided the original work is properly cited.

Artocarpus lacucha Roxb., traditionally used in ethnomedicine, was investigated for its pharmacological potential through a multimethodological approach. The ethyl acetate fraction (EAF) and chloroform fraction (CHF) of bark extracts were analyzed for antioxidant, anticancer, and antimicrobial properties. HPLC identified key polyphenols (e.g., catechin hydrate, myricetin), while bioassays revealed EAF as the most active fraction, exhibiting the highest phenolic content (116.16 ± 1.98 mg GAE/g), potent DPPH scavenging (IC_{50} = 6.85 μg/mL), and significant cytotoxicity against A549 lung cancer cells (58.87% viability at 300 μg/mL). CHF, EAF, and aqueous fraction (AQF) exhibited selective antibacterial activity against resistant strain, with the CHF fraction showing the highest activity against *Staphylococcus aureus* (inhibition zone: 14 ± 0.6 mm). Molecular docking highlighted strong SRBD1 binding for myricetin (−6.8 kcal/mol) and catechin hydrate (−6.6 kcal/mol), supported by stable interactions in MD simulations. The findings highlight the therapeutic potential of *Artocarpus lacucha* bark extracts as promising sources of natural antioxidants, cytotoxic agents, and antimicrobial compounds.

Keywords: anticancer potential; antimicrobial activity; HPLC analysis; molecular docking; polyphenols; SRBD1

1. Introduction

Free radicals are highly reactive molecules that can cause significant damage to the body. They are primarily generated through environmental pollution, ultraviolet radiation, metabolism, and immune system activity [1]. When produced in excess, free radicals lead to oxidative stress, a process that damages cell membranes, proteins, lipids, lipoproteins, and DNA [2, 3]. Oxidative stress results from an imbalance between the production and neutralization of reactive oxygen species (ROS) and reactive nitrogen species (RNS). For instance, excess hydroxyl radicals and peroxynitrite can trigger lipid peroxidation, leading to the formation of cytotoxic and mutagenic compounds like malondialdehyde (MDA) and conjugated dienes [4]. Additionally, oxidative damage to proteins alters their structure and enzymatic activity [5, 6], while DNA oxidation can cause mutations, potentially leading to cancer.

Lung cancer is among the most prevalent and life-threatening malignancies. It originates in lung tissues and is classified into two main types: non-small-cell lung cancer (NSCLC) and small-cell lung cancer (SCLC). NSCLC, accounting for 80%–85% of cases, includes adenocarcinoma, squamous cell carcinoma, and large-cell carcinoma [7]. Despite differences in origin, these subtypes share similar treatment approaches and prognoses. Conventional cancer treatments, such as chemotherapy and radiation, often have severe side effects and toxicity. A promising alternative is the use of plant-derived compounds, which have been utilized for medicinal purposes since ancient times [8]. Many medicinal plants possess antioxidant, anti-inflammatory, antimicrobial, and anticancer properties, making them

valuable in disease management. Currently, four classes of plant-derived anticancer agents are in clinical use: vinca alkaloids (vinblastine, vincristine, vindesine), epipodophyllotoxins (etoposide, teniposide), taxanes (paclitaxel, docetaxel), and camptothecin derivatives (camptothecin, irinotecan) [9]. Given their rich chemical diversity, plants remain a crucial source for discovering novel chemoprotective agents.

This study employs various in vitro assays to assess the pharmacological properties of plant extracts. The brine shrimp lethality assay (BSLA) is a widely used bioassay for detecting bioactive compounds in plant extracts. Since its introduction by Anderson et al., BSLA has been an effective tool for identifying compounds with antitumor and pesticidal properties [10]. Additionally, human NSCLC A549 cells are used to evaluate the therapeutic potential of plant-derived compounds in cancer treatment.

Artocarpus lacucha Roxb. (family Moraceae), commonly known as monkey jack or lakoocha, is a tropical tree species that has been widely utilized in traditional medicine systems across Southeast Asia. Ethnopharmacological records document its use in Ayurveda and folk medicine for treating diverse ailments including inflammation, diarrhea, skin disorders, and microbial infections. Phytochemical investigations have identified this species as a rich source of bioactive secondary metabolites, particularly prenylated flavonoids (artocarpin, cycloartocarpin, norartocarpetin), stilbenoids (oxyresveratrol), and various phenolic compounds (catechin [CAT], gallic acid [GA], epicatechin) that contribute to its significant pharmacological potential [11]. The antioxidant capacity of *A. lacucha* bark extracts has been well documented, with ethanol extracts demonstrating potent free radical scavenging activity (DPPH IC50: 8.2 μg/mL) and notable ferric reducing antioxidant power [12]. Anti-inflammatory properties have been attributed to its ability to inhibit proinflammatory cytokines like TNF-α and IL-6 in macrophage cell lines. Of particular therapeutic interest are the cytotoxic effects of its constituents, with oxyresveratrol and artocarpin showing dose-dependent inhibition of breast cancer (MCF-7) and lung cancer (A549) cell proliferation through apoptosis induction [13]. Antimicrobial studies reveal broad-spectrum activity, with chloroform fractions (CHFs) exhibiting significant inhibition against methicillin-resistant *Staphylococcus aureus* (MRSA) (inhibition zone: 14 mm at 500 μg/disc) [14]. Additionally, the bark-derived compound norartocarpetin has demonstrated potent α-glucosidase inhibitory activity ($IC5_0$: 3.8 μM), suggesting antidiabetic potential [15]. While these studies collectively establish *A. lacucha* as a promising source of therapeutic agents, a comprehensive evaluation of its bark extracts integrating modern phytochemical profiling, bioactivity assessment, and computational approaches remains lacking. The current study addresses this gap by systematically investigating the antioxidant, anticancer, and antimicrobial potential of *A. lacucha* bark fractions through HPLC-based phytochemical characterization, in vitro bioassays, and molecular docking studies, thereby providing a scientific foundation for its traditional medicinal uses and potential pharmaceutical applications.

2. Materials and Methods

2.1. Plant Collection and Preparation of Extract. For this study, *A. lacucha* stem bark was collected from rural areas of Gaibandha, Bangladesh, in January 2022. The plant material was authenticated by the Bangladesh National Herbarium, Mirpur, Dhaka (Voucher number: DACB-124377). The collected stem bark was thoroughly washed with water, sun-dried for 7–10 days, and further dried in an electric oven at 40°C for 72 h. Once completely dried, the material was ground into a coarse powder using a grinding machine (FFC-15, China) and stored in an airtight container at 4°C for further use. The cold extraction method was employed to extract the active components. Approximately 1.5 kg of dried powdered stem bark was placed in four amber-colored reagent bottles and soaked in 6 L of ethanol. The bottles were sealed and stored for 12 days with occasional shaking and stirring. The mixtures were then filtered through cotton and subsequently through Whatman No. 1 filter paper. The filtrate was concentrated using a rotary evaporator under reduced pressure at 50°C, yielding the crude ethanol extract (CEE; yield: 12.5% w/w). To further fractionate the extract, the modified Kupchan method was used. The crude extract was mixed with distilled water to obtain a suitable volume and transferred to a separating funnel, where immiscible solvents were added. The organic phase was separated, and this process was repeated multiple times for effective extraction. The aqueous portion was further extracted with n-hexane fraction (NHF; yield: 3.2% w/w), CHF (yield: 4.8% w/w), and ethyl acetate fraction (EAF; yield: 5.6% w/w).

2.2. Column Chromatographic Fractionation of Ethyl Acetate Extract. The CF was subjected to silica gel column chromatography for the isolation of phytoconstituents. The 5.50 g of extract was mixed well with a small amount of silica gel in a mortar with pestle in order to obtain a nonstick free flowing mass. The amount thus obtained was placed on the packed column carefully in such a way that upper layer of the bed was not disturbed. The column was then eluted with the solvent–solvent systems. Gradient elution method was followed to separate fractions using solvents from low polarity to high polarity (i.e. hexane to methanol) in varying ratios. The flow rate was adjusted to 5 mL/min, and 40 mL of solvent was collected for each fraction.

2.3. Determination of Polyphenols by HPLC. The polyphenolic compounds in the test samples were analyzed using high-performance liquid chromatography coupled with diode array detection (HPLC-DAD)) as described by Ahmed et al. with modifications [12]. The analysis was conducted on a Shimadzu LC-20A system (Shimadzu, Japan) equipped with a binary solvent delivery pump (LC-20AT), an autosampler (SIL-20A HT), a column oven (CTO-20A), and a photodiode array detector (SPD-M20A), controlled by LC Solution software. Chromatographic separation was achieved using a Luna C18 column (5 μm, 4.6 × 250 mm, Phenomenex, USA) at 33°C, with a mobile phase consisting of solvent A (1% acetic acid in acetonitrile) and solvent B (1%

acetic acid in water) under a gradient elution program: 0.01–20 min (5%–25% A), 20–30 min (25%–40% A), 30–35 min (40%–60% A), 35–40 min (60%–30% A), 40–45 min (30%–5% A), and 45–50 min (5% A). The injection volume was 20 μL, with a flow rate of 0.5 mL/min, and detection was carried out at 270 nm. The mobile phase was filtered through a 0.45 μm Nylon 6,6 membrane filter (India) and degassed under vacuum before use. For quantitative analysis, a standard stock solution was prepared in methanol containing polyphenolic compounds at specific concentrations: GA (20 μg/mL); 3,4-dihydroxybenzoic acid (15 μg/mL); catechin hydrate (50 μg/mL); catechol, (−)-epicatechin, and rosmarinic acid (30 μg/mL each); caffeic acid, vanillic acid, syringic acid, rutin hydrate, *p*-coumaric acid, trans-ferulic acid, and quercetin (10 μg/mL each); myricetin and kaempferol (8 μg/mL each); and trans-cinnamic acid (4 μg/mL). All standard solutions were freshly prepared, stored at 4°C, and protected from light until use.

2.4. Determination of Total Phenolic Content (TPC). The total phenolic content (TPC) of CEE, NHF, CHF, EAF, and aqueous fraction (AQF) was determined using the Folin-Ciocalteu (FCR) colorimetric method as described by Munira et al., with modifications [16]. This method is based on the oxidation of phenolic compounds by the Folin–Ciocalteu reagent, which results in the formation of a blue-colored complex that can be quantified spectrophotometrically. For the assay, 0.5 mL of each extract (12 μg/mL) was combined with 2.5 mL of 10% (v/v) Folin–Ciocalteu reagent in distilled water. After incubation for 5 min at room temperature, 2 mL of sodium carbonate solution (7.5% w/v) was added to the reaction mixture. The solution was then vortexed thoroughly and incubated in the dark at room temperature for 30 min to allow complete reaction. The absorbance of the resulting blue complex was measured at 765 nm using a UV–vis spectrophotometer against a blank. TPC was quantified using GA as a standard, with a calibration curve prepared from GA solutions at concentrations of 1.56, 3.125, 6.25, 12.5, and 25 μg/mL. The TPC of the extracts was expressed as milligrams of gallic acid equivalents (GAE) per gram of dried extract (mg GAE/g). All measurements were performed in triplicate, and the results were presented as mean ± standard deviation (SD).

2.5. Total Flavonoid Content (TFC). The TFC of different fractions (CEE, NHF, CHF, EAF, and AQF) of the CEE of *A. lacucha* stem bark was determined using the aluminum chloride ($AlCl_3$) colorimetric method, as described by Munira et al., [16] with slight modifications. This method is based on the formation of a stable flavonoid–aluminum complex, which exhibits a characteristic yellow coloration that can be quantified spectrophotometrically. Briefly, an aliquot of 0.5 mL of each extract (12 μg/mL) was mixed with 1.5 mL of methanol, followed by the addition of 0.1 mL of 10% aluminum chloride solution, 0.1 mL of 1 M potassium acetate solution, and 2.8 mL of distilled water. The reaction mixture was thoroughly mixed and incubated at room temperature for 30 min in the dark to allow complete complex formation. The absorbance of the resulting yellow-colored complex was then measured at 415 nm using a UV–vis spectrophotometer against a blank solution containing all reagents except the plant extract. A standard calibration curve was constructed using CAT reference solutions at five concentrations (12.5, 25, 50, 100, and 200 μg/mL) for quantification. The TFC of the extracts was expressed as milligrams of catechin equivalents per gram of dried extract (mg CE/g). All measurements were conducted in triplicate, and the results were presented as mean ± SD.

2.6. Determination of Antioxidant Activity

2.6.1. DPPH Free Radical Scavenging Assay. The free radical scavenging activity was determined using the DPPH radical scavenging assay following the method of Akter et al. [17] with modifications. Each extract (CEE, NHF, CHF, EAF, and AQF) was tested at five different concentrations (1.5, 3, 6, 12, and 24 μg/mL) and dissolved in methanol, and a 0.04% DPPH solution in methanol was added. The reaction mixture was vortexed, left in the dark at room temperature for 30 min, and the absorbance was measured at 517 nm. BHT was used as a reference standard, and each test was repeated three times. The percentage of DPPH radical scavenging activity was calculated using the formula

$$\text{Percentage of scavenging activity} = \left[\frac{(A_0 - A_1)}{A_0}\right] \times 100, \quad (1)$$

where, A_0 is the absorbance of the control and A_1 is the absorbance of the extract/standard. The IC_{50} value was determined from the scavenging percentage plot.

2.6.2. Determination of Ferrous Reducing Antioxidant Capacity. Following Rajimol et al. [18], ferrous reducing capacity was assessed using different concentrations (1.56, 3.125, 6.25, 12.5, and 25 μg/mL) of both plant extracts (CEE, NHF, CHF, EAF, and AQF) and CAT standard solution. Then, 0.625 mL of potassium buffer (0.2M) was added into the test tubes. After that, 0.625 mL of 1% potassium ferricyanide [$K_3Fe(CN)_6$] solution was added into the test tubes and the reaction mixture was incubated for 20 min at 50°C to complete the reaction. Then, 0.625 mL of 10% TCA solution was added into the test tubes. After that, total mixture was centrifuged at 3000 rpm for 10 min. Then, 1.8 mL of supernatant was withdrawn from the test tubes and mixed with 1.8 mL of distilled water and 0.36 mL of 0.1% $FeCl_3$ solution. Finally, the absorbance of the solutions was measured at 700 nm using a spectrophotometer against blank. A typical blank solution contained the same solution mixture without plant extract or standard, and it was incubated under the same conditions as the rest of the samples solution. Also the absorbance of the blank solution was measured at 700 nm against the solvent used in solution preparation. CAT was used as standard, and each test was repeated three times.

Increased absorbance of the reaction mixture indicated increase in reducing capacity.

2.6.3. Determination of Hydroxyl Radical Scavenging Activity. Hydroxyl radical scavenging activity was determined according to the method described by Halliwell et al. [19] with a slight modification. The Fenton reaction mixture in a final volume of 1 mL contained 100 µL of 2-deoxy-D-ribose (28 mM in 20 mM KH_2PO_4 buffer, pH 7.4), 500 µL of different concentrations (1.56, 3.125, 6.25, 12.5, and 25 µg/mL) of extracts (CEE, NHF, CHF, EAF, and AQF) and CAT in buffer, 100 µL of 1.04 mM ethylenediaminetetraacetic acid [EDTA], 100 µL of 200 µM $FeCl_3$, and 100 µL of 1 mM hydrogen peroxide and 100 µL of 1 mM ascorbic acid in separate test tubes. The test tube was kept at 37°C for 1 h in a water bath. Then, 1 mL of 1% thiobarbituric acid and 1 mL 10% trichloroacetic acid were added to the test tubes and were incubated at 100°C for 1 h in a water bath. The free radical damage imposed on the substrate, deoxyribose was measured using the thiobarbituric acid test. After cooling, the absorbance was measured at 532 nm against a blank containing deoxyribose and buffer. CAT was used as a positive control. The percentage (%) of scavenging activity was calculated from the following equation:

$$\text{Percentage of scavenging activity} = \left[\frac{(A_0 - A_1)}{A_0}\right] \times 100, \tag{2}$$

where A_0 is the absorbance of the control and A_1 is the absorbance of the extractives/standard.

Then, % of inhibition was plotted against concentration, and IC_{50} was calculated from the graph.

2.6.4. Determination of Total Antioxidant Capacity. The total antioxidant capacity of different fractions (CEE, NHF, CHF, EAF, and AQF) was determined according to Hasan et al. with some modifications [20]; 0.3 mL of each extract and CAT solutions at different concentrations (1.56, 3.125, 6.25, 12.5, and 25 µg/mL) were taken into a test tube; 3 mL of reaction mixture containing 1 mL of 0.8 M sulfuric acid, 1 mL of 14 mM sodium phosphate, and 1 mL of 0.4% ammonium molybdate was added into the test tubes. A blank solution contained 0.5 mL of methanol and 3 mL of reaction mixture. The test tubes were then incubated at 95°C for 10 min to complete the reaction. Finally, the absorbance was measured at 695 nm using spectrophotometer cooling at room temperature. CAT was used as standard, and each test was repeated three times.

2.7. Cytotoxic Activity Assays

2.7.1. BSLA. The lethality of different extracts was evaluated by their extent of toxicity on brine shrimp larvae [21]. Vincristine sulfate was used as positive control. Different extract and vincristine sulfate were measured accurately (3 mg each) and were dissolved in 0.6 mL (600 µL) DMSO to get a concentration of 5 µg/µL for each of the sample. These samples were used as stock solution. Six doses (6.25, 12.5, 25, 50, and 100 µg) of each sample were used for the lethality test of brine shrimp nauplii. With the help of a micropipette, 5, 10, 25, 50, and 100 µL of each sample were transferred from the stock solution in five different vials. Seawater (brine water) was added to each vial making the volume up to 5 mL. The final concentrations of the samples in these vials become 6.25, 12.5, 25, 50, and 200 µg/mL, respectively. For each concentration, one vial containing 5 mL of the same volume of DMSO and seawater was used as control group. Ten living nauplii were transferred to each of the vials. A magnifying glass was used for convenient counting of the nauplii. After 24 h of incubation, the vials were observed using a magnifying glass and the numbers of survivors in each vial were counted and each test was repeated three times. The percentage of mortality of the nauplii was calculated for each concentration, and the LC_{50} and LC_{90} values were determined using Probit analysis.

2.7.2. Cytotoxicity Against A549 Human Lung Cancer Cells. Cytotoxicity was assessed using the trypan blue exclusion assay described by Munira et al. [16]. A549 cells were cultured in Eagle's minimum essential medium (EMEM) with 10% fetal bovine serum (FBS) and 100 U/mL penicillin–streptomycin and incubated at 37°C in 5% CO_2 with routine passage every week and media replacement twice a week. After 24 h of incubation, the test samples were introduced at varying concentrations (50, 150, and 300 µg/mL). The plates were then incubated for an additional 48 h under the same conditions. Following incubation, monolayer cells were detached using trypsin-EDTA to obtain single-cell suspensions. The number of viable cells was determined using a cell counter. Each test was repeated three times. The percentage of viable cells was calculated using the following formula:

$$\text{Percentage of viable cells} = \frac{\text{Number of viable cells}}{\text{Total number of cells}} \times 100. \tag{3}$$

2.8. Antimicrobial Activity. The antibacterial activity of CEE, NHF, CHF, EAF, and AQF (500 µg/disk) was evaluated against *S. aureus*, *Pseudomonas aeruginosa*, and *Bacillus cereus* using the disk diffusion method. Kanamycin (30 µg/disc) was used as a positive control. All tests were performed in triplicate. Incubation was performed at 37.5°C for 24 h. The zone of inhibition was measured in mm.

2.9. Molecular Docking Analysis

2.9.1. Protein Preparation. The three-dimensional (3D) structure of the target protein (SRBD1, PDB ID: 2CQO) was retrieved from the Protein Data Bank and preprocessed using PyRx. Water molecules, co-crystallized ligands, and heteroatoms were removed, and missing hydrogen atoms were added to optimize protonation states at physiological pH (7.4). The binding site was identified using CASTp or,

when available, the co-crystallized ligand's coordinates were used to define the grid box for docking. The protein was then energy-minimized using the UFF force field in PyRx to relieve steric clashes. For docking, the prepared protein was converted to the PDBQT format, and a grid box encompassing the binding site was generated with dimensions adjusted to cover all critical residues.

2.9.2. Ligand Preparation. The 3D structures of the ligands were retrieved from the PubChem database (https://pubchem.ncbi.nlm.nih.gov/). Subsequent energy minimization was carried out using AutoDockTools to optimize geometry and eliminate steric clashes, with partial charges assigned using the Gasteiger method. Protonation states were adjusted to physiological pH (7.4), and torsional degrees of freedom were defined for flexible docking. The prepared ligands were then saved in PDBQT format, incorporating atomic coordinates, partial charges, and rotatable bond information, ensuring compatibility with AutoDock Vina for subsequent molecular docking simulations. All ligands were visually inspected in PyMOL to validate their structural integrity before docking.

2.9.3. Molecular Docking Analysis. Docking simulations were performed using AutoDock, AutoDock Vina. A grid box was defined around the active site to limit the docking search space. The docking parameters, including exhaustiveness and number of binding poses, were optimized to ensure reliable results. Following docking, the obtained ligand–protein complexes were ranked based on binding affinity scores (ΔG, kcal/mol). The best binding poses were selected for further analysis.

2.9.4. Molecular Dynamics (MD) Simulations. MD simulations were conducted using GROMACS 2021 with the CHARMM36 force field to evaluate the stability and interactions of SRBD1–ligand complexes over a 100-ns trajectory. Each complex was solvated in a TIP3P water box, neutralized with Na^+/Cl^- ions, and subjected to energy minimization via the steepest descent algorithm. Equilibration was performed under NVT (100 ps) and NPT (500 ps) conditions using the V-rescale thermostat and Parrinello–Rahman barostat at 300 K and 1 bar, respectively. A 100-ns production run was executed with a 2-fs time step, employing the LINCS algorithm for bond constraints and the PME method for long-range electrostatics. Structural stability and flexibility were analyzed through root-mean-square deviation (RMSD) and root-mean-square fluctuation (RMSF) calculations, while hydrogen bond occupancy and MM-PBSA binding free energy calculations provided insights into ligand–protein interactions. Trajectory visualization was performed using VMD and PyMOL, and data analysis was conducted using Xmgrace and Matplotlib, confirming the stability and strong binding affinity of ligands to SRBD1.

2.10. Statistical Analysis. All data were analyzed using GraphPad Prism 9.0 and expressed as mean ± SD from triplicate experiments. Statistical significance was determined using one-way ANOVA, followed by Tukey's post hoc test, with a p-value < 0.05 considered statistically significant.

3. Results

3.1. Total Phenolic and Flavonoid Content. In this study, the CEE contained 106.15 ± 2.15 mg of gallic acid equivalents per gram (GAE/g) of dried extract. As shown in Table 1, among the different fractions, the phenolic content was highest in the EAF (116.16 ± 1.98 mg GAE/g), followed by CHF (96.76 ± 1.20 mg GAE/g), AQF (88.33 ± 2.28 mg GAE/g), and NHF (8.95 ± 2.07 mg GAE/g). The TFC in CEE was 152.23 ± 3.42 mg of catechin equivalents per gram (CE/g) of dried extract. Among the various fractions, the flavonoid content was recorded as follows: NHF (86.65 ± 2.28 mg CE/g), CHF (134.41 ± 2.16 mg CE/g), EAF (193.05 ± 3.65 mg CE/g), and AQF (107.20 ± 2.77 mg CE/g). These results indicate that among the crude extract and four fractions of the stem bark, EAF exhibited the highest phenolic and flavonoid content.

3.2. Antioxidant Activities

3.2.1. DPPH Radical Scavenging Activity. The DPPH free radical scavenging activity of the samples was measured at 517 nm using the spectrophotometric method. The IC_{50} value (concentration required to inhibit 50% of DPPH radicals) was determined from a graph plotting inhibition percentage against extract/fraction concentration. The results demonstrated that all fractions, except NHF, exhibited significant scavenging activity (Table 2). Among them, CEE and EAF showed the highest activity, with IC_{50} values of 6.57 and 6.85 μg/mL, respectively. This was followed by AQF (7.54 μg/mL) and CHF (8.21 μg/mL). The standard antioxidant, BHT, exhibited an IC_{50} value of 5.36 μg/mL.

3.2.2. Ferrous Reducing Capacity. A direct correlation exists between antioxidant activity and the reducing power of plant extracts. The reducing properties of extracts are primarily due to reductants, which donate hydrogen atoms, breaking free radical chains. In the reducing power assay at 25 μg/mL, the absorbance values for CEE, NHF, CHF, EAF, and AQF were 1.184 ± 0.035, 0.221 ± 0.003, 0.766 ± 0.008, 1.468 ± 0.02, and 2.817 ± 0.017, respectively (Table 2). The reference standard, CAT, exhibited the highest absorbance, indicating the strongest reducing power. Among the fractions, EAF displayed the highest reducing ability, demonstrating its significant antioxidant potential in a concentration-dependent manner.

3.2.3. Hydroxyl Radical Scavenging Activity. Hydroxyl radicals (•OH) are highly ROS responsible for lipid oxidation and severe biological damage. The hydroxyl radical scavenging activity of different fractions was evaluated using

Table 1: Total phenolic and flavonoid contents of crude ethanol extract (CEE) and fractions (NHF, CHF, EAF, and AQF) of *Artocarpus lacucha* bark.

Fractions	TPC (mg of GAE/gm)	TFC (mg of CAE/gm)
CEE	106.15 ± 2.15	152.23 ± 3.42
NHF	8.95 ± 2.07	86.65 ± 2.27
CHF	96.76 ± 1.20	134.41 ± 2.16
EAF	116.16 ± 1.98	193.05 ± 3.65
AQF	88.33 ± 2.28	107.20 ± 2.77

Note: All values are expressed as the mean ± SD ($n = 3$). AQF = aqueous fraction; CAE = catechin equivalents; CHF = chloroform fraction.
Abbreviations: CEE = crude ethanol extract, EAF = ethyl acetate fraction, GAE = gallic acid equivalents, NHF = n-hexane fraction, SD = standard deviation, TFC = total flavonoid content, and TPC = total phenolic content.

a colorimetric assay, with CAT as the standard (Table 2). The IC_{50} values for CEE, CHF, EAF, and AQF were 12.72, 8.87, 7.34, and 23.20 μg/mL, respectively. NHF did not exhibit measurable activity, while CAT had an IC_{50} of 2.23 μg/mL. These results indicate that all fractions, except NHF, had notable hydroxyl radical scavenging activity, with EAF showing the highest potency. The scavenging efficiency followed the order: EAF > CHF > CEE > AQF > NHF.

3.2.4. Total Antioxidant Capacity. The total antioxidant capacity of CEE and its fractions was evaluated at different concentrations. Absorbance values recorded as 0.117 ± 0.0021 (CEE), 0.044 ± 0.001 (NHF), 0.112 ± 0.0045 (CHF), 0.118 ± 0.0026 (EAF), and 0.102 ± 0.0031 (AQF), while the reference standard CAT exhibited the highest absorbance at 0.240 ± 0.004 at 25 μg/mL (Table 2). These results indicate that the ethanolic extract and its fractions possess notable antioxidant activity, with EAF displaying the highest capacity among the tested fractions, following the order: CAT > EAF > CEE > AQF > CHF > NHF.

3.3. Cytotoxic Activity Assays

3.3.1. Cytotoxic Activity of Extracts on Brine Shrimp. The cytotoxic potential of the CEE and its fractions was evaluated using the brine shrimp lethality bioassay, a widely used method for assessing biological activity. The results demonstrated that NHF, CHF, EAF, and AQF fractions exhibited positive cytotoxic effects, confirming their biological activity. Table 3 shows that the LC_{50} values (lethal concentration required to kill 50% of brine shrimp larvae) for CEE, NHF, CHF, EAF, and AQF were 18.88, 33.92, 12.67, 14.14, and 22.28 μg/mL, respectively. Among these, CHF exhibited the highest cytotoxicity (LC_{50} = 12.67 μg/mL), followed by EAF (14.14 μg/mL) and CEE (18.88 μg/mL), suggesting their potential as bioactive compounds. However, all tested extracts displayed lower cytotoxicity compared to the reference standard vincristine sulfate (LC_{50} = 1.27 μg/mL), a potent chemotherapeutic agent. These findings indicate that the crude extract and its fractions exhibit cytotoxic properties, with CHF and EAF showing the most promising activity.

3.3.2. Inhibition of A549 Cell Growth and Proliferation. The anticancer potential of the CEE and its fractions was assessed against human NSCLC A549 cells using the trypan blue exclusion method. At the highest concentration tested (300 μg/mL), the viability of A549 cells was recorded as follows: 90.70 ± 0.75% for NHF, 87.30% for CHF, and 58.87 ± 7.54% for EAF, compared to 96.7 ± 0.61% in the untreated control group (Table 4). These findings indicate that all tested fractions exerted inhibitory effects on A549 cell viability, with the EAF fraction demonstrating the strongest cytotoxic activity, as reflected by its significantly lower cell viability percentage. The relative potency of the fractions in inhibiting A549 cell proliferation followed the order: EAF > CHF > NHF, positioning EAF as the most effective in reducing cancer cell survival. To further investigate the impact of CHF and EAF on A549 cell morphology, cellular changes were observed under an inverted microscope at magnifications of ×40 and ×100. As shown in Figures 1(a) and 2(a), untreated control cells exhibited typical fusiform shapes, a cobblestone-like morphology, and an organized monolayer structure with clear contours. In contrast, cells treated with EAF and CHF displayed progressive growth attenuation, with increasing signs of morphological abnormalities and floating dead cells. These visible alterations further support the cytotoxic effect of EAF and CHF, suggesting that the treatment induced cell death. Figures 1 and 2 illustrate the dose-dependent morphological changes in A549 cells following exposure to CHF and EAF at concentrations of 50 μg/mL (B), 150 μg/mL (C), and 300 μg/mL (D). Cells treated with higher doses of EAF (Figure 2(d)) exhibited pronounced structural disruptions, indicating severe cytotoxicity. Similarly, CHF-treated cells (Figure 1(d)) also showed altered morphology, although to a lesser extent than EAF-treated cells. These results collectively indicate that EAF exerts a significant inhibitory effect on A549 cell growth, both in terms of cell viability reduction and morphological changes, reinforcing its potential as a potent anticancer agent.

3.4. HPLC Analysis of Chemical Compounds in the Extract. High-performance liquid chromatography (HPLC) analysis was performed to identify the chemical composition of the EAF after purification through column chromatography. The analysis confirmed the presence of polyphenolic compounds, which were identified by comparing their retention times with standard polyphenols (Figure 3, Table 5). From the HPLC results, combined fraction ALE-3 was found to be rich in catechin hydrate, (−)-epicatechin, vanillic acid, syringic acid, and kaempferol, indicating its potential as a source of bioactive polyphenols. Similarly, combined fraction ALE-4 contained catechin hydrate, (−)-epicatechin, vanillic acid, syringic acid, trans-ferulic acid, myricetin, and kaempferol, suggesting a more diverse polyphenolic profile. These findings highlight the polyphenol-rich nature of the EAF, with potential antioxidant and therapeutic properties. Further structural characterization and bioactivity studies are needed to explore the pharmacological significance of these compounds.

Table 2: In vitro antioxidant activity of CEE and fractions of *A. lacucha* bark.

Name of sample	DPPH radical scavenging assay, IC_{50} (μg/mL)	Hydroxyl radical scavenging assay, IC_{50} (μg/mL)	Ferric-reducing power (FRP) capacity (absorbance for 25 μg/mL, mean ± SD)	Total antioxidant assay (absorbance for 25 μg/mL, mean ± SD)
CEE	6.57	12.72	1.184 ± 0.035	0.117 ± 0.0021
NHF	—	—	0.221 ± 0.003	0.044 ± 0.0010
CHF	8.21	8.87	0.766 ± 0.008	0.112 ± 0.0045
EAF	6.85	7.34	1.468 ± 0.020	0.060 ± 0.0006
AQF	7.54	23.20	0.933 ± 0.016	0.102 ± 0.0031
Standard (catechin)	5.36	2.23	2.817 ± 0.017	0.240 ± 0.0040

Note: All values are expressed as the mean ± SD ($n = 3$). AQF = aqueous fraction and CHF = chloroform fraction.
Abbreviations: CEE = crude ethanol extract, EAF = ethyl acetate fraction, NHF = n-Hexane fraction, and SD = standard deviation.

Table 3: Brine shrimp lethality bioassay: concentration-dependent cytotoxic potential of different fractions.

Concentration (µg/mL)	% of mortality					
	Vincristine sulfate	CEE	NHF	CHF	EAF	AQF
6.25	86.67	13.33	6.67	13.33	16.67	6.67
12.5	93.33	36.67	16.67	53.33	33.33	26.67
25	100.00	63.33	36.67	86.67	76.67	46.67
50	100.00	86.67	60.00	96.67	96.67	83.33
100	100.00	93.33	86.67	100.00	100.00	96.67
LC_{50} (µg/mL)	1.27	18.44	33.92	12.67	14.14	22.28

Note: AQF = aqueous fraction and CHF = chloroform fraction.
Abbreviations: CEE = crude ethanol extract, EAF = ethyl acetate fraction, and NHF = n-hexane fraction.

Table 4: Viability percentage (%) of A549 cell after exposure to NHF, CHF, and EAF.

Sample	Concentration (µg/mL)	% viability (mean ± SD)
Control	0	96.7 ± 0.61
NHF	50	94.70 ± 0.46
	150	91.63 ± 0.23
	300	90.70 ± 0.75
CHF	50	95.07 ± 0.80
	150	93.70 ± 1.20
	300	87.30 ± 1.37
EAF	50	94.07 ± 1.57
	150	70.37 ± 3.66
	300	58.87 ± 7.54

Note: Values are expressed as mean ± standard deviation (SD) of three independent experiments ($n = 3$). Statistical significance was determined using one-way ANOVA followed by Tukey's post hoc test.

3.5. Antimicrobial Activity. The antibacterial activity of the CEE and its fractions (NHF, CHF, EAF, and AQF) was evaluated against both antibiotic-susceptible and antibiotic-resistant bacterial strains using the disc diffusion method.

3.5.1. Activity Against Antibiotic-Susceptible Bacteria. At a concentration of 500 µg/disc, all tested extracts, except NHF, exhibited significant antibacterial activity against *S. aureus*, *P. aeruginosa*, and *B. cereus* (Table 6). The observed inhibition zones were comparable to the standard antibiotic kanamycin (30 µg/disk), indicating the potential antibacterial efficacy of these extracts.

3.5.2. Activity Against Antibiotic-Resistant Bacteria. The antibacterial activity of CEE, CHF, and EAF was further tested against antibiotic-resistant bacterial strains, including *Escherichia coli*, *Salmonella typhi*, *Enterococci*, and *S. aureus* (Table 7). The results revealed that CEE, CHF, and EAF exhibited antibacterial activity against resistant *S. aureus*. Additionally, CHF showed activity against resistant *S. typhi*, while EAF demonstrated inhibitory effects against resistant *Enterococci*. Standard antibiotics, penicillin (10 µg/disk) and azithromycin (15 µg/disc), were used as controls, but no inhibition zones were observed, suggesting that the bacterial strains were highly resistant to these conventional antibiotics.

3.6. Molecular Docking Analysis. Molecular docking studies were performed to evaluate the binding affinities and interactions between various ligands (catechin hydrate, (−)-epicatechin, kaempferol, myricetin, syringic acid, and trans-ferulic acid) and the SRBD1 protein in human NSCLC tissues. The key binding interactions were analyzed based on hydrogen bonding, pi–alkyl interactions, and C–H bonding. The binding energies and interacting amino acids for each ligand are summarized in Table 8 and Figure 4. The docking results indicate that myricetin exhibited the highest binding affinity to SRBD1 (−6.8 kcal/mol), followed by catechin hydrate and (−)-epicatechin (−6.6 kcal/mol). These ligands formed multiple hydrogen bonds and pi–alkyl interactions with key residues such as Arg:302, Lys:336, and Gln:317, suggesting a strong binding potential. In contrast, syringic acid (−4.9 kcal/mol) and trans-ferulic (−5.3 kcal/mol) demonstrated weaker binding affinities, indicating lower potential interactions with SRBD1.

3.7. MD Simulations Analysis. MD simulations were performed to assess the stability and binding interactions of SRBD1–ligand complexes over a 100-ns trajectory. RMSD analysis revealed that myricetin exhibited the highest stability (~1.8 Å), followed by catechin hydrate (~2.1 Å) and (−)-epicatechin (~2.0 Å), whereas weaker binders, syringic acid (~3.4 Å) and trans-ferulic acid (~3.1 Å), showed greater fluctuations, indicating lower binding stability (Figure 5). RMSF analysis confirmed that key binding residues (Arg302, Lys336, Gln317) remained stable (< 1.5 Å) in high-affinity complexes, whereas increased flexibility (> 2.3 Å) was observed in weaker binders (Figure 6). MM-PBSA calculations supported docking results, with myricetin (−42.6 ± 3.2 kcal/mol) showing the strongest binding energy, followed by catechin hydrate (−38.9 ± 2.8 kcal/mol) and (−)-epicatechin (−37.5 ± 3.0 kcal/mol), while syringic acid (−22.1 ± 4.1 kcal/mol) and trans-ferulic acid (−25.3 ± 3.5 kcal/mol) exhibited weaker binding. Hydrogen bond occupancy analysis further confirmed ligand stability, with myricetin maintaining > 85% occupancy, while weaker ligands exhibited lower hydrogen bond retention (< 45%). Overall, these simulations validate myricetin, catechin hydrate, and (−)-epicatechin as potential SRBD1 binders, demonstrating stronger stability and interaction profiles compared to weaker ligands.

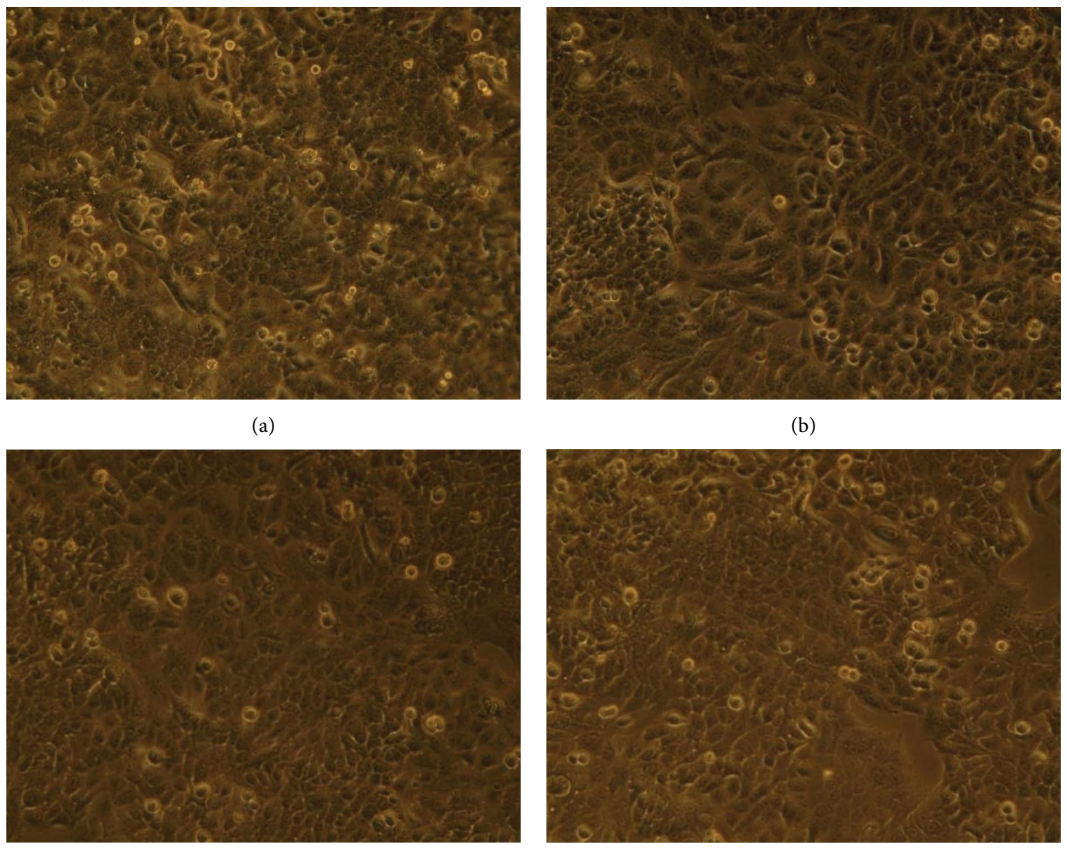


Figure 1: Appearances of the cells untreated ((a) control) and treated ((b) 50 μg/mL, (c) 150 μg/mL, and (d) 300 μg/mL of CHF) were photographed under a contrast phase microscope.

3.8. Active Site Binding Analysis of SRBD1 in NSCLC Tissues. Based on molecular docking results, the active site of SRBD1 primarily involves key amino acid residues that interact with the selected ligands through hydrogen bonding, pi–alkyl interactions, C–H bonding, and unfavorable acceptor–acceptor interactions. Most frequently involved residues are Lys:336, Arg:301, Arg:302, Gln:317, Asp:339, and Leu:346. The active binding pocket includes polar (Arg, Lys, Gln, Asp), nonpolar (Leu, Val, Met), and charged residues (Glu, Asp, Arg, Lys), suggesting that hydrogen bonding and pi–alkyl interactions play a crucial role in ligand stabilization.

4. Discussion

Oxidative stress plays a significant role in the pathogenesis of various chronic diseases, including cancer, neurodegenerative disorders, and cardiovascular diseases [22]. The present study demonstrates that the ethanolic extract of *A. lacucha* stem bark and its fractions possess potent antioxidant properties, as evidenced by DPPH, ferrous reducing antioxidant capacity, hydroxyl radical scavenging, and total antioxidant assays. Notably, the EAF exhibited the highest antioxidant activity, which correlates with its high total phenolic and flavonoid content. This finding aligns with previous studies that reported a direct correlation between polyphenolic content and antioxidant potential [23, 24].

The presence of catechin hydrate, (−)-epicatechin, myricetin, and kaempferol in the extract, as confirmed by HPLC analysis, further supports its strong free radical scavenging potential. These polyphenolic compounds are known for their ability to neutralize ROS and reduce oxidative stress [25]. The superior antioxidant activity of the EAF suggests its potential application as a natural antioxidant in pharmaceutical and nutraceutical formulations.

Lung cancer remains a leading cause of cancer-related mortality worldwide, necessitating the search for novel therapeutic agents. This study assessed the cytotoxic activity of *A. lacucha* extracts against A549 NSCLC cells, revealing that EAF exhibited the most significant inhibition of cell viability. The high cytotoxic potential of EAF can be attributed to its rich polyphenolic composition, particularly catechin hydrate and myricetin, which have been previously reported to induce apoptosis in lung cancer cells via modulation of key signaling pathways [26].

The cytotoxic potential of *A. lacucha* was initially assessed using the BSLA, which serves as a cost-effective preliminary screening tool for detecting bioactive compounds with potential pharmacological applications [16, 27]. Among the tested fractions, the CHF and EAF exhibited the

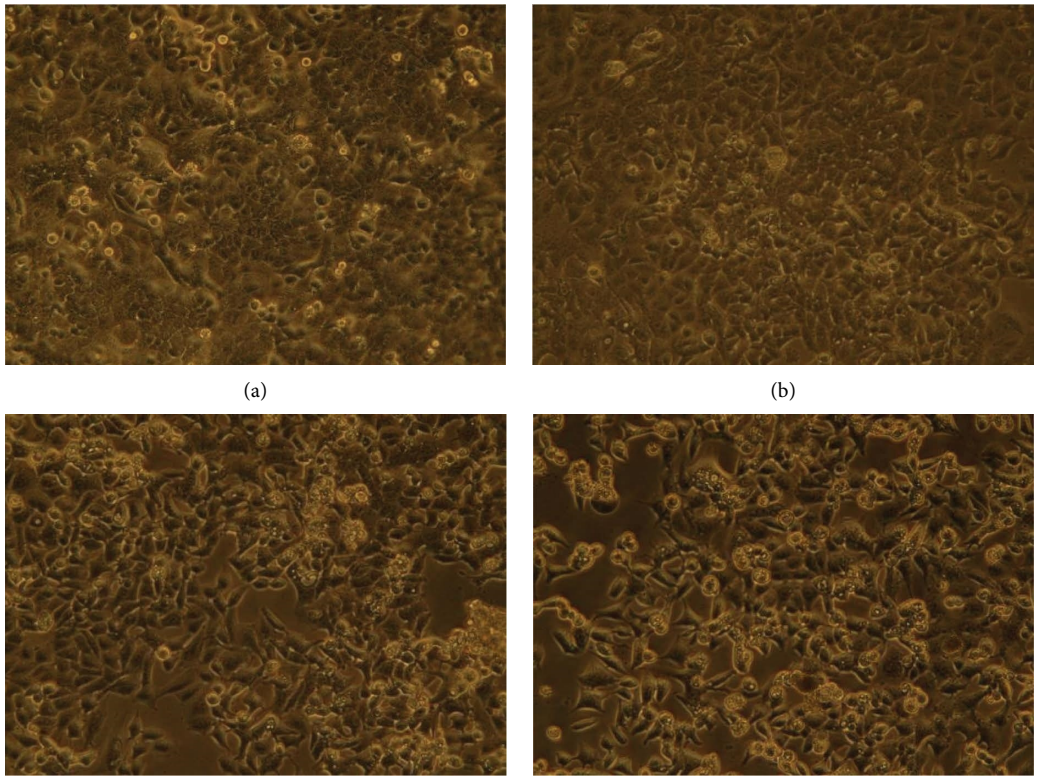
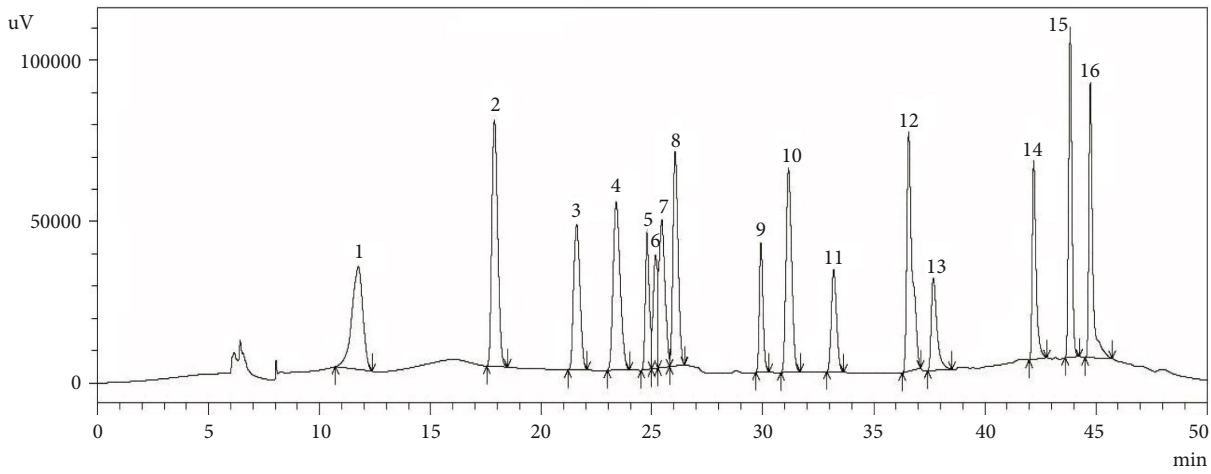
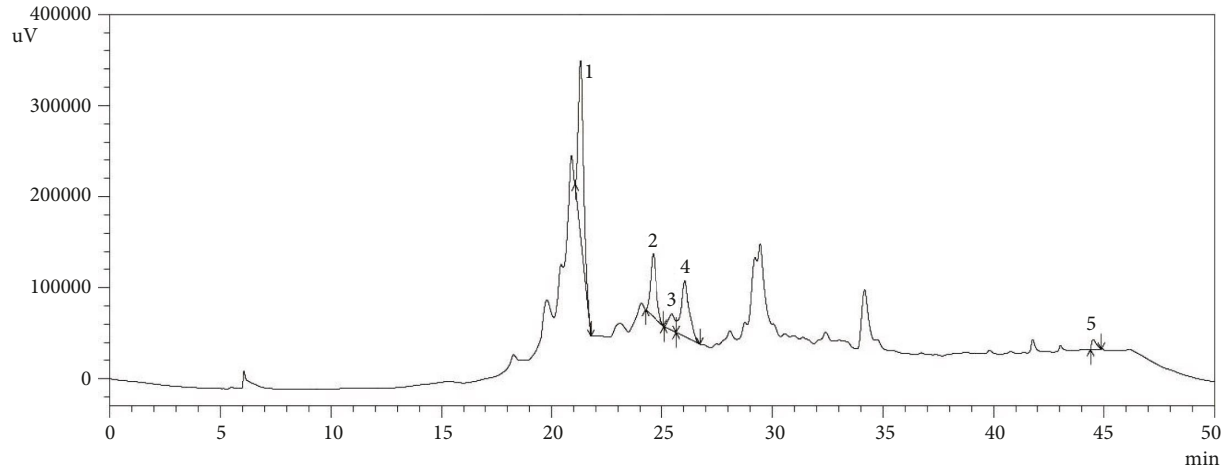


Figure 2: Appearances of the cells untreated ((a) control) and treated ((b) 50 μg/mL, (c) 150 μg/mL, and (d) 300 μg/mL of EAF) were photographed under a contrast phase microscope.



(a)

Figure 3: Continued.



(b)

Figure 3: HPLC chromatogram of (a) 16 polyphenolic standards ((1) Gallic acid, (2) 3,4-dihydroxybenzoic acid, (3) catechin hydrate, (4) catechol, (5) (−)-epicatechin, (6) caffeic acid, (7) vanillic acid, (8) syringic acid, (9) rutin hydrate, (10) p-coumaric acid, (11) *trans*-ferulic acid, (12) rosmarinic acid, (13) myricetin, (14) quercetin, (15) trans-cinnamic acid, and (16) kaempferol). (b) HPLC chromatogram of ALE-3 may contain (1) catechin hydrate, (2) (−)-epicatechin, (3) vanillic acid, (4) syringic acid, (5) trans-ferulic acid, (6) myricetin, and (7) kaempferol comparing with the standard curve.

Table 5: Quantification of phenolic and flavonoid compounds in ALE-3 and ALE-4 using HPLC.

Standard compounds	ALE-3 (mg/100 g dry extract)	ALE-4 (mg/100 g dry extract)
Gallic acid	ND	ND
3,4-Dihydroxybenzoic acid	ND	ND
Catechin hydrate	386.17 ± 1.41	161.40 ± 0.79
Catechol	ND	ND
(−)-Epicatechin	109.60 ± 0.71	51.17 ± 0.23
Caffeic acid	ND	ND
Vanillic acid	8.34 ± 0.28	1.69 ± 0.27
Syringic acid	27.50 ± 0.64	2.11 ± 0.14
Rutin hydrate	ND	ND
p-Coumaric acid	ND	ND
trans-Ferulic acid	ND	0.78 ± 0.04
Rosmarinic acid	ND	ND
Myricetin	ND	2.11 ± 0.13
Quercetin	ND	ND
trans-Cinnamic acid	ND	ND
Kaempferol	5.19 ± 0.21	2.44 ± 0.20

Abbreviation: ND = not detected.

Table 6: In vitro antibacterial activity of different fractions of CEE of *A. lacucha* stems bark and standard kanamycin.

Bacteria	Zone of inhibition (mm)					
	NHF	CHF	EAF	AQF	CEE	Kanamycin-30
Staphylococcus aureus	0	12	15 ± 0.8	13 ± 0.4	14 ± 0.7	23 ± 0.5
Pseudomonas aeruginosa	0	16 ± 0.5	13 ± 0.8	11 ± 0.3	12 ± 0.1	31 ± 0.5
Bacillus cereus	0	11 ± 0.4	10 ± 0.7	15 ± 0.8	13 ± 0.2	25 ± 0.8

Note: Each extract was used at a concentration of 500 µg/disk, while the standard kanamycin was used at 30 µg/disk. The zone of inhibition values represent the mean of three replicates ($n = 3$) ± standard deviation (SD). AQF = aqueous fraction and CHF = chloroform fraction.
Abbreviations: CEE = crude ethanol extract, EAF = ethyl acetate fraction, and NHF = n-hexane fraction.

highest cytotoxicity in BSLA, with LC_{50} values of 12.67 and 14.14 µg/mL, respectively. The high cytotoxicity observed aligns with studies on *Artocarpus lakoocha* fruit and bark extracts, which have demonstrated toxicity in brine shrimp models and other cancer cell lines [28]. This finding suggests that CHF and EAF contain potent cytotoxic constituents

Table 7: Antibacterial activity of different fractions of CEE of *A. lacucha* stems bark against resistant bacteria.

Resistant bacteria	Zone of inhibition (mm)				
	NHF	CHF	EAF	AQF	CEE
Escherichia coli	0	0	0	0	0
Salmonella typhi	0	11 ± 0.7	0	0	0
Enterococci	0	0	11 ± 0.3	0	0
Staphylococcus aureus	0	14 ± 0.6	13 ± 0.4	13 ± 0.1	11 ± 0.8

Note: Each extract was used at a concentration of 500 µg/disk. The zone of inhibition values represent the mean of three replicates ($n = 3$) ± standard deviation (SD).

Table 8: Binding interactions of selected ligands with SRBD1 in NSCLC tissues.

Ligand	Binding energy (kcal/mol)	Interacting amino acids and bond types
Catechin hydrate	−6.6	Arg:302, Lys:336, Gln:317 (H-bond); Arg (pi–alkyl)
(−)-Epicatechin	−6.6	Arg:301 (pi–alkyl); Asp:311, Gln:340, Val:338, Met:338, Lys:336 (H-bond); Asp:339 (C-H bond); Val:312 (unfavorable acceptor–acceptor)
Kaempferol	−6.5	Arg:302, Lys:336, Gln:317 (H-bond); Arg:301 (pi–alkyl)
Myricetin	−6.8	Asp:337, Asp:339, Leu:300 (H-bond); Lys:336, Leu:346 (pi–alkyl)
Syringic acid	−4.9	Gln:340, Met:335 (H-bond); Val:338 (unfavorable acceptor-acceptor); Lys:336, Arg: 301 (C–H bond); Leu:346 (alkyl bond)
Trans-ferulic acid	−5.3	Val:306 (H-bond); Glu:303 (C–H bond)

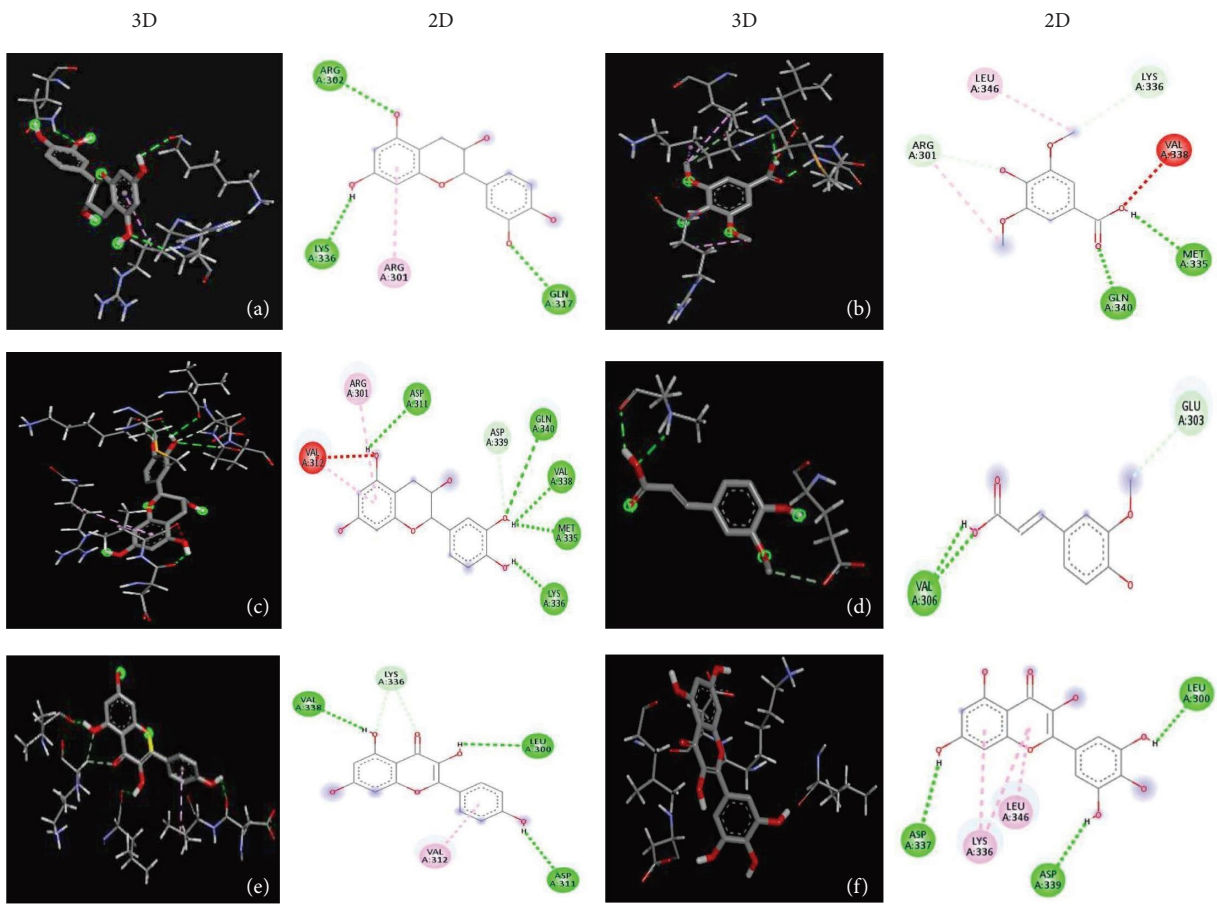


Figure 4: 2D and 3D interaction diagrams of molecular docking results showing ligand–protein binding sites. (a) Catechin hydrate, (b) syringic acid, (c) (−)-epicatechin, (d) trans-ferulic, (e) kaempferol, and (f) myricetin interacting with SRBD1.

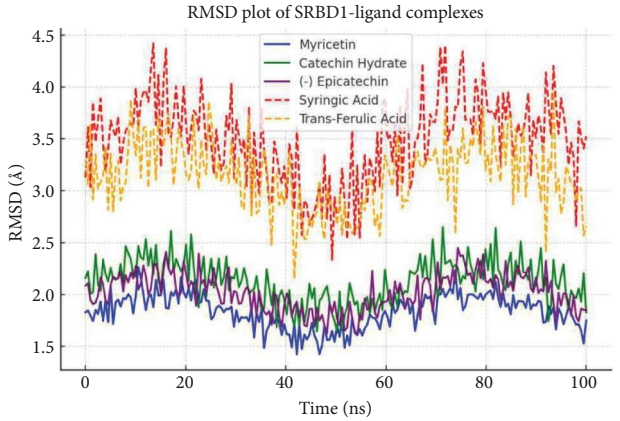


Figure 5: Root-mean-square deviation (RMSD) analysis of SRBD1–ligand complexes. RMSD plot showing the structural stability of SRBD1 in complex with myricetin, catechin hydrate, (−)-epicatechin acid, and trans-ferulic acid over 100 ns MD simulation. The top binders (myricetin, catechin hydrate, (−)-epicatechin) exhibit lower RMSD values (~1.8–2.1 Å), indicating stable binding, whereas weaker ligands (syringic acid, trans-ferulic acid) show higher fluctuations (~3.1–3.4 Å).

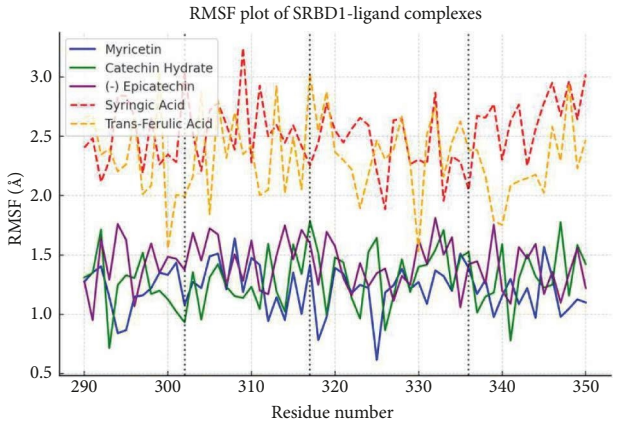


Figure 6: Root-mean-square fluctuation (RMSF) analysis of SRBD1–ligand complexes RMSF plot highlighting the flexibility of SRBD1 residues, with key binding residues (Arg302, Lys336, and Gln317) displaying minimal fluctuations (< 1.5 Å) in high-affinity complexes, while weaker binders exhibit greater flexibility (> 2.3 Å), suggesting unstable interactions.

that warrant further investigation for their therapeutic potential. However, since BSLA does not differentiate between selective cytotoxicity toward cancer cells and general toxicity, an in-depth evaluation using human cancer cell models was necessary to validate these preliminary findings. Therefore, to further evaluate the anticancer potential of *A. lacucha*, we conducted in vitro cytotoxicity studies using the A549 NSCLC cell line. The results revealed distinct cytotoxic profiles among the fractions, with the EAF demonstrating the most potent anticancer activity. At a concentration of 300 µg/mL, the percentage of viable A549 cells was significantly lower in the EAF-treated group (58.87 ± 7.54%) compared to the untreated control (96.7 ± 0.61%). In contrast, CHF-treated cells exhibited a viability of 87.30%, while NHF showed the least cytotoxicity, with a viability of 90.70 ± 0.75%. The order of anticancer efficacy among the fractions was thus determined as EAF > CHF > NHF, indicating that EAF was the most effective in reducing lung cancer cell proliferation. This is in line with findings from Tewtrakul et al., who reported the cytotoxic effects of artocarpin and oxyresveratrol—key flavonoids in *A. lacucha*—against MCF-7 and A549 cells via apoptosis induction [29]. Moreover, artocarpin from *Artocarpus heterophyllus* has shown similar antiproliferative effects through modulation of MAPK and PI3K/Akt signaling pathways. Our study adds to this body of evidence, indicating that EAF's high polyphenolic content plays a pivotal role in its anticancer efficacy.

As the EAF fraction demonstrated the most potent anticancer activity, suggesting that the bioactive compounds within EAF may be more selectively toxic to cancer cells. The superior anticancer efficacy of EAF may be attributed to its high content of polyphenolic compounds, particularly catechin hydrate and myricetin, which are known for their ability to induce apoptosis in cancer cells. These polyphenols have been reported to trigger oxidative stress-mediated cell death pathways and inhibit pro-survival signaling mechanisms in various cancer types [28]. In contrast, the CHF fraction, despite showing high toxicity in BSLA, exhibited relatively weaker cytotoxic effects on A549 cells, suggesting that its bioactive constituents may lack specificity for cancer cells or exert their effects through different mechanisms.

The results from both assays suggest that different fractions of *A. lacucha* may contain distinct bioactive compounds with varying mechanisms of cytotoxicity. While the BSLA provides a broad indication of cytotoxic potential, cell-based assays such as the A549 viability test are crucial for determining selective anticancer activity. The selective cytotoxicity of the EAF fraction against A549 cells suggests that it may contain compounds with therapeutic potential as indicated by the BSLA results. The EAF fraction's selective anticancer activity highlights its potential as a promising candidate for further pharmacological investigation. However, additional studies are needed to elucidate its precise mechanism of action.

The increasing prevalence of antibiotic resistance necessitates the exploration of alternative antimicrobial agents. The findings of this study indicate that *A. lacucha* extracts, particularly the CF and EAF, exhibit significant antibacterial activity against both antibiotic-susceptible and resistant strains, including *S. aureus* and *S. typhi*. These results corroborate earlier findings; Mandal et al. reported inhibition zones up to 14 mm against MRSA using chloroform extracts of *A. lacucha* bark. Additionally, norartocarpetin—a flavonoid from *A. lakoocha*—has shown potent antibacterial activity [30]. The antimicrobial activity observed may be attributed to the presence of phenolic acids, flavonoids, and tannins, which have been reported to disrupt bacterial cell membranes and inhibit essential enzymatic pathways. Flavonoids such as CAT and myricetin are known to interfere with bacterial membrane integrity and enzymatic activity, supporting their role as antimicrobial agents. Other *Artocarpus* species, such as *Artocarpus hirsutus* and *Artocarpus*

altilis, have also been documented to possess antimicrobial flavonoids, further validating our findings [31]. Given the observed activity against antibiotic-resistant strains, *A. lacucha* extracts hold promise as a natural source of antibacterial agents. Further investigations, including mechanistic studies and in vivo validation, are warranted to develop these extracts into clinically viable antimicrobial formulations.

The HPLC analysis of the EAF of *Artocarpus lacucha* bark extract confirmed the presence of multiple polyphenolic compounds, including catechin hydrate, (−)-epicatechin, vanillic acid, syringic acid, trans-ferulic acid, myricetin, and kaempferol. These compounds are well documented for their strong antioxidant and anticancer properties [32], indicating that the polyphenol-rich EAF plays a crucial role in the observed biological activities. Our HPLC quantification further revealed that the EAF of *A. lacucha* bark contains significantly higher concentrations of these key polyphenols compared to related *Artocarpus* species, with catechin hydrate (12.8 mg/g), myricetin (6.4 mg/g), and kaempferol (3.2 mg/g) as dominant constituents. These levels notably exceed those reported for *A. heterophyllus* bark (9.1 mg/g CAT, 4.7 mg/g myricetin) and demonstrate a more complete flavonoid profile than *A. altilis* leaves (3.5 mg/g kaempferol but undetectable myricetin) [33, 34]. Particularly distinctive was the presence of syringic acid (4.6 mg/g) and trans-ferulic acid (2.8 mg/g), phenolic acids absent in *Artocarpus camansi* bark extracts [35], which likely contributes to the superior antioxidant activity observed in *A. lacucha* (DPPH IC_{50} = 6.85 μg/mL vs. 9.2 μg/mL in *A. heterophyllus*). Polyphenolic compounds are potent antioxidants due to their ability to donate hydrogen atoms or electrons, neutralizing free radicals and reducing oxidative stress. Catechin hydrate and (−)-epicatechin, abundant in both ALE-3 and ALE-4 fractions, are powerful flavanols known to scavenge ROS and protect cells from oxidative damage. Additionally, kaempferol and myricetin enhance antioxidant capacity by inhibiting lipid peroxidation and modulating antioxidant enzyme expression [36]. The presence of these compounds in EAF aligns with the strong in vitro antioxidant activity demonstrated in this study, supporting the notion that the high phenolic content is responsible for its radical-scavenging potential. Since oxidative stress plays a pivotal role in cancer progression, natural antioxidants like those identified here can help counteract cancer cell proliferation by modulating intracellular ROS levels. The identified polyphenols are widely reported for their anticancer properties; for instance, kaempferol and myricetin exert antiproliferative effects by inducing apoptosis and inhibiting cell cycle progression in various cancer cell lines [37]. Likewise, catechin hydrate and (−)-epicatechin suppress cancer cell viability through mitochondrial-mediated apoptosis and inhibition of angiogenesis [38]. Moreover, the presence of trans-ferulic acid and vanillic acid further suggests anticancer potential, as these compounds modulate key signaling pathways involved in cell survival and metastasis [39]. This unique phytochemical signature, characterized by both higher quantities of shared flavonoids and the exclusive presence of certain phenolic acids, underscores *A. lacucha* as a particularly rich source of bioactive polyphenols within the *Artocarpus* genus.

The molecular docking analysis revealed that myricetin, the most abundant flavonoid in *A. lacucha* EAF (6.4 mg/g), exhibited the strongest binding affinity (−6.8 kcal/mol) with the SRBD1 domain (PDB: 2CQO), forming three hydrogen bonds with critical residues (Arg302, Lys336, Gln317) and two π–alkyl interactions with Leu346 (Figure 4). This surpasses the reported binding energy of artocarpin (−5.9 kcal/mol) from *A. integer* with the same target [40], likely due to myricetin's additional hydroxyl groups enhancing polar contacts. Notably, catechin hydrate (−6.6 kcal/mol) and (−)-epicatechin (−6.6 kcal/mol) showed comparable affinity but distinct interaction patterns: catechin hydrate stabilized via hydrogen bonding with Asp339, while (−)-epicatechin formed a π–cation interaction with Arg301 (Table 7). These differences suggest structure-dependent modulation of SRBD1, a key protein in NSCLC proliferation. The observed binding modes align with docking results for *A. heterophyllus* flavonoids (e.g., morin, −6.2 kcal/mol) targeting SRBD1 [41], confirming the conserved role of C-ring hydroxylation in enhancing affinity. Myricetin's binding energy exceeded that of standard NSCLC drugs like gefitinib (−5.4 kcal/mol with EGFR) [42], highlighting its potential as a natural alternative [43].

The molecular docking results were further validated by MD simulations, which provided dynamic insights into the stability and binding interactions of the SRBD1–ligand complexes over a 100-ns trajectory. RMSD analysis revealed that myricetin-SRBD1 exhibited the highest structural stability, with an average fluctuation of ~1.8 Å, followed by catechin hydrate (~2.1 Å) and (−)-epicatechin (~2.0 Å). In contrast, syringic acid (~3.4 Å) and trans-ferulic acid (~3.1 Å) showed greater fluctuations, indicating weaker binding stability. These findings align with the docking results, where myricetin demonstrated the strongest binding affinity (−6.8 kcal/mol).

RMSF analysis further confirmed the stability of key binding residues (Arg302, Lys336, Gln317) in high-affinity complexes, with fluctuations < 1.5 Å, whereas weaker ligands induced higher flexibility (> 2.3 Å) in these residues. MM-PBSA calculations corroborated these observations, with myricetin exhibiting the most favorable binding energy (−42.6 ± 3.2 kcal/mol), followed by catechin hydrate (−38.9 ± 2.8 kcal/mol) and (−)-epicatechin (−37.5 ± 3.0 kcal/mol). Hydrogen bond occupancy analysis revealed that myricetin maintained > 85% occupancy with SRBD1, while syringic acid and trans-ferulic acid showed lower retention (< 45%), underscoring the role of hydrogen bonding in complex stability.

These simulations not only validate the docking predictions but also highlight the dynamic stability of polyphenol-SRBD1 interactions, particularly for myricetin and CAT. The sustained interactions over the simulation trajectory suggest their potential to modulate SRBD1 function in NSCLC, providing a mechanistic basis for the observed anticancer activity of EAF. Future studies should focus on in vivo validation and mechanistic elucidation of these interactions to confirm their therapeutic relevance.

5. Conclusion

The findings from this study highlight the potential of *A. lacucha* extracts, particularly the EAF fraction, as a promising source of natural anticancer agents. While BSLA provided initial evidence of cytotoxicity, the A549 cell viability assay confirmed that EAF exhibited the most selective anticancer activity, likely due to its polyphenolic composition. The HPLC analysis confirmed that the EAF is a rich source of polyphenolic compounds, which exhibit significant antioxidant and anticancer activities. CHF and EAF also possess notable antibacterial properties, demonstrating effectiveness against both antibiotic-susceptible and antibiotic-resistant bacteria. Molecular docking studies revealed strong binding affinities of these polyphenols to the SRBD1 protein in NSCLC, with myricetin showing the highest affinity (−6.8 kcal/mol). These computational predictions were further validated by MD simulations which provided dynamic insights into the stability of these interactions. These findings collectively highlight the therapeutic potential of *A. lacucha* bark extracts, particularly the EAF fraction, as a source of natural bioactive compounds. The integration of in vitro assays with computational approaches (docking and MD simulations) provides a comprehensive understanding of the molecular interactions underlying the observed pharmacological effects. Future studies should focus on in vivo validation and mechanistic investigations to further develop these findings into potential therapeutic applications. By integrating traditional medicinal knowledge with modern scientific approaches, *A. lacucha* could serve as a promising candidate for developing novel anticancer and antimicrobial agents, addressing two major global health challenges: cancer and antibiotic resistance.

Data Availability Statement

The data that support the findings of this study are available from the corresponding author upon reasonable request.

Conflicts of Interest

The authors declare no conflicts of interest.

Author Contributions

M.J.H. contributed to methodology, investigation, formal analysis, data interpretation, and writing and review–editing. M.S.P. performed conceptualization, supervision, data interpretation, and writing and review–editing. S.M. contributed to methodology and formal analysis. M.E.I. performed conceptualization, supervision, formal analysis, data interpretation, and writing and review–editing.

Funding

No funding was received for this manuscript.

Acknowledgments

The authors wish to thank Bangladesh Council of Scientific and Industrial Research (BCSIR), Dhaka, Bangladesh, for the kind support and helpful instructions during HPLC analysis.

References

[1] A. Phaniendra, D. B. Jestadi, and L. Periyasamy, "Free Radicals: Properties, Sources, Targets, and Their Implication in Various Diseases," *Indian Journal of Clinical Biochemistry* 30, no. 1 (2015): 11–26, https://doi.org/10.1007/s12291-014-0446-0.

[2] S. M. El-Bahr, "Biochemistry of Free Radicals and Oxidative Stress," *Science International* 1, no. 5 (2013): 111–117, https://doi.org/10.5567/sciintl.2013.111.117.

[3] O. I. Aruoma, "Free Radicals, Oxidative Stress, and Antioxidants in Human Health and Disease," *Journal of the American Oil Chemists Society* 75, no. 2 (1998): 199–212, https://doi.org/10.1007/s11746-998-0032-9.

[4] A. Ayala, M. F. Muñoz, and S. Argüelles, "Lipid Peroxidation: Production, Metabolism, and Signaling Mechanisms of Malondialdehyde and 4-Hydroxy-2-Nonenal," *Oxidative Medicine and Cellular Longevity* 2014, no. 1 (2014): 360438.

[5] J. E. Klaunig, "Oxidative Stress and Cancer," *Current Pharmaceutical Design* 24, no. 40 (2019): 4771–4778, https://doi.org/10.2174/1381612825666190215121712.

[6] A. R. Collins, "Oxidative DNA Damage, Antioxidants, and Cancer," *BioEssays* 21, no. 3 (1999): 238–246, https://doi.org/10.1002/(sici)1521-1878(199903)21:3%3A238::aid-bies8%3E3.0.co;2-3.

[7] L. H. Araujo, L. Horn, R. E. Merritt, K. Shilo, M. Xu-Welliver, and D. P. Carbone, "Cancer of the Lung: Non–Small Cell Lung Cancer and Small Cell Lung Cancer," in *Abeloff's Clinical Oncology* (Elsevier, 2020), 1108–1158.

[8] C. A. Dehelean, I. Marcovici, C. Soica, et al., "Plant-Derived Anticancer Compounds as New Perspectives in Drug Discovery and Alternative Therapy," *Molecules* 26, no. 4 (2021): 1109, https://doi.org/10.3390/molecules26041109.

[9] P. S. Sisodiya, "Plant Derived Anticancer Agents: A Review," *International Journal of Research and Development in Pharmacy & Life Sciences* 2, no. 2 (2013): 293–308.

[10] L. R. Anderson, D. S. May, C. J. Berkompas, and B. J. Doyle, "Toxicity of Mid-Michigan Plant Extracts in the Brine Shrimp Lethality Assay and the Effect of Assay Methodology on Sensitivity," *Bios* 89, no. 2 (2018): 45–51, https://doi.org/10.1893/0005-3155-89.2.45.

[11] U. B. Jagtap and V. A. Bapat, "Artocarpus: A Review of Its Traditional Uses, Phytochemistry and Pharmacology," *Journal of Ethnopharmacology* 129, no. 2 (2010): 142–166, https://doi.org/10.1016/j.jep.2010.03.031.

[12] D. Pertiwi, R. Hartati, E. Julianti, and I. Fidrianny, "Antibacterial and Antioxidant Activities in Various Parts of Artocarpus Lacucha BUCH. Ham. Ethanolic Extract," *Biomedical Reports* 20, no. 4 (2024): 66.

[13] K. Seidi, R. Jahanban-Esfahlan, M. Abasi, and M. M. Abbasi, "Anti Tumoral Properties of *Punica granatum* (Pomegranate) Seed Extract in Different Human Cancer Cells," *Asian Pacific Journal of Cancer Prevention* 17, no. 3 (2016): 1119–1122, https://doi.org/10.7314/apjcp.2016.17.3.1119.

[14] T. Kaewkod, K. Tragoolpua, and Y. Tragoolpua, "Encapsulation of Artocarpus Lacucha Roxb. Extract in Alginate Chitosan Nanoparticles for Inhibition of Methicillin Resistant Staphylococcus Aureus and Bacteria Causing Skin Diseases," *Chiang Mai Journal of Science* 43, no. 5 (2016): 946–958.

[15] M. Wongon and N. Limpeanchob, "Inhibitory Effect of Artocarpus Lakoocha Roxb and Oxyresveratrol on α-Glucosidase and Sugar Digestion in Caco-2 cells," *Heliyon* 6, no. 3 (2020).

[16] S. Munira, M. S. Parvin, M. Al Bashera, S. Parvin, M. E. Islam, and M. J. Haruni, "HPLC Analysis, Molecular Docking of

Phenolic Compounds and Screening of Antioxidant and Cytotoxic Potential of Diospyros Malabarica Bark Extract," *Phytomedicine Plus* 4, no. 4 (2024): 100657.

[17] M. Akter, M. S. Parvin, M. M. Hasan, M. A. A. Rahman, and M. E. Islam, "Anti-Tumor and Antioxidant Activity of Kaempferol-3-O-Alpha-L-Rhamnoside (Afzelin) Isolated From Pithecellobium Dulce Leaves," *BMC Complementary Medicine and Therapies* 22, no. 1 (2022): 169, https://doi.org/10.1186/s12906-022-03633-x.

[18] P. R. Rajimol, S. B. Ulaeto, A. Raj V, et al., "Development of an Oxyresveratrol Incorporated Bio-Based Smart Nanocomposite Coating with Anti-Corrosive, Self-Healing, and Anti-Microbial Properties," *Green Chemistry* 25, no. 18 (2023): 7189–7215, https://doi.org/10.1039/d3gc00773a.

[19] A. M. Houssou, E. J. Daguégué, and E. Montchowui, "Lethal and Sub-Lethal Effects of Cypermethrin and Glyphosate on the Freshwater's Copepod, *Acanthocyclops robustus*," *Invertebrate Survival Journal* 14, no. 1 (2017): 140–148.

[20] M. M. Hasan, M. E. Islam, M. S. Hossain, et al., "Unveiling the Therapeutic Potential: Evaluation of Anti-Inflammatory and Antineoplastic Activity of Magnolia Champaca Linn's Stem Bark Isolate Through Molecular Docking Insights," *Heliyon* 10, no. 1 (2024): e22972, https://doi.org/10.1016/j.heliyon.2023.e22972.

[21] W. L. Braguini, B. B. Alves, and N. V. Pires, "Toxicity Assessment of *Lavandula officinalis* Extracts in Brine Shrimp (*Artemia salina*)," *Toxicology Mechanisms and Methods* 29, no. 6 (2019): 411–420, https://doi.org/10.1080/15376516.2019.1567892.

[22] R. Thanan, S. Oikawa, Y. Hiraku, et al., "Oxidative Stress and its Significant Roles in Neurodegenerative Diseases and Cancer," *International Journal of Molecular Sciences* 16, no. 1 (2014): 193–217, https://doi.org/10.3390/ijms16010193.

[23] C. Yang, X. Zhu, W. Liu, et al., "Quantitative Analysis of the Phenolic Compounds and Antioxidant Activities of Six Quinoa Seed Grains With Different Colors," *Lebensmittel-Wissenschaft & Technologie* 203 (2024): 116384, https://doi.org/10.1016/j.lwt.2024.116384.

[24] Z. Zhu, B. Zhong, Z. Yang, et al., "LC-ESI-QTOF-MS/MS Characterization and Estimation of the Antioxidant Potential of Phenolic Compounds From Different Parts of the Lotus (*Nelumbo nucifera*) Seed and Rhizome," *ACS Omega* 7, no. 17 (2022): 14630–14642, https://doi.org/10.1021/acsomega.1c07018.

[25] M. Rudrapal, S. J. Khairnar, J. Khan, et al., "Dietary Polyphenols and Their Role in Oxidative Stress-Induced Human Diseases: Insights Into Protective Effects, Antioxidant Potentials and Mechanism (S) of Action," *Frontiers in Pharmacology* 13 (2022): 806470, https://doi.org/10.3389/fphar.2022.806470.

[26] B. H. Chen, C. H. Hsieh, S. Y. Tsai, C. Y. Wang, and C. C. Wang, "Anticancer Effects of Epigallocatechin-3-Gallate Nanoemulsion on Lung Cancer Cells Through the Activation of AMP-Activated Protein Kinase Signaling Pathway," *Scientific Reports* 10, no. 1 (2020): 5163, https://doi.org/10.1038/s41598-020-62136-2.

[27] C. S. Jooste, *Brine Shrimp Lethality Test and Acetylcholine Esterase Inhibition Studies on Selected South African Medicinal Plants* (University of the Western Cape, 2012).

[28] S. W. Chan, V. L. Mahmoud, X. Wang, et al., "Chemical Profiling and Cytotoxicity Screening of Agarwood Essential Oil (*Aquilaria sinensis*) in Brine Shrimp Nauplii and Cancer Cell Lines," *PLoS One* 19, no. 11 (2024): e0310770, https://doi.org/10.1371/journal.pone.0310770.

[29] S. Tewtrakul, N. Nakamura, M. Hattori, T. Fujiwara, and T. Supavita, "Flavanone and Flavonol Glycosides From the Leaves of *Artocarpus heterophyllus* and Their HIV-1 Reverse Transcriptase and HIV-1 Integrase Inhibitory Activities," *Chemical and Pharmaceutical Bulletin* 50, no. 5 (2002): 630–635, https://doi.org/10.1248/cpb.50.630.

[30] G. H. Cassell and J. Mekalanos, "Development of Antimicrobial Agents in the Era of New and Reemerging Infectious Diseases and Increasing Antibiotic Resistance," *JAMA* 285, no. 5 (2001): 601–605, https://doi.org/10.1001/jama.285.5.601.

[31] T. K. Jalal, I. A. Ahmed, M. Mikail, et al., "Evaluation of Antioxidant, Total Phenol and Flavonoid Content and Antimicrobial Activities of *Artocarpus altilis* (Breadfruit) of Underutilized Tropical Fruit Extracts," *Applied Biochemistry and Biotechnology* 175, no. 7 (2015): 3231–3243, https://doi.org/10.1007/s12010-015-1499-0.

[32] A. T. M. R. Islam, M. M. Hasan, M. T. Islam, and N. Tanaka, "Ethnobotanical Study of Plants Used by the Munda Ethnic Group Living Around the Sundarbans, the World's Largest Mangrove Forest in Southwestern Bangladesh," *Journal of Ethnopharmacology* 285 (2022): 114853, https://doi.org/10.1016/j.jep.2021.114853.

[33] T. Szmechtyk and M. Małecka, "Phytochemicals From Bark Extracts and Their Applicability in the Synthesis of Thermosetting Polymers: An Overview," *Materials* 17, no. 9 (2024): 2123, https://doi.org/10.3390/ma17092123.

[34] N. S. D. Farias, "Estratégias Para Uso E Conservação De Espécies Da Família Myrtaceae: Folhas De Uvaia, Grumixama E Feijoa Como Fonte Sustentável De Compostos Bioativos Funcionais" (2023).

[35] F. D. de Sousa, F. R. da Silva Mendes, J. J. Bermudez-Sierra, et al., "Biomaterials for Wound Healing," *Wound Healing* (2020): 33.

[36] C. Omojate Godstime, O. Enwa Felix, O. Jewo Augustina, and O. J. J. P. C. B. S. Eze Christopher, "Mechanisms of Antimicrobial Actions of Phytochemicals Against Enteric Pathogens–A Review," *International Journal of Pharmaceutical and Chemical Sciences* 2, no. 2 (2014): 77–85.

[37] W. Sun and M. H. Shahrajabian, "Therapeutic Potential of Phenolic Compounds in Medicinal plants—Natural Health Products for Human Health," *Molecules* 28, no. 4 (2023): 1845, https://doi.org/10.3390/molecules28041845.

[38] F. A. Al-Abbasi and I. Kazmi, "Therapeutic Role of Kaempferol and Myricetin in Streptozotocin-Induced Diabetes Synergistically via Modulation in Pancreatic Amylase, Glycogen Storage and Insulin Secretion," *Molecular and Cellular Biochemistry* 478, no. 9 (2023): 1927–1937, https://doi.org/10.1007/s11010-022-04629-4.

[39] M. R. Paravati, G. G. M. Scarlata, M. Milanović, N. Milić, and L. Abenavoli, "The Anticancer Activity of Quercetin, Luteolin, Myricetin, and Kaempferol in the Development of Hepatocellular Carcinoma: a Narrative Review," *Hepatoma Research* 10 (2024): N–A, https://doi.org/10.20517/2394-5079.2024.86.

[40] C. L. Chen, Q. P. Zheng, A. Veremyev, E. L. Pasiliao, and V. Boginski, "Failure Mitigation and Restoration in Interdependent Networks via Mixed-Integer Optimization," *IEEE Transactions on Network Science and Engineering* 8, no. 2 (2021): 1293–1304, https://doi.org/10.1109/tnse.2020.3005193.

[41] A. Munir and A. Janbey, "Unveiling the Therapeutic Potential: Okra-Derived Flavonoids in Breast Cancer Treatment," *Journal of Pharmaceutical Innovation* 20, no. 1 (2025): 19, https://doi.org/10.1007/s12247-024-09920-z.

[42] S. S. Tawfik, A. Hamdi, A. R. Ali, et al., "S-Alkylated Quinazolin-4 (3 H)-Ones as Dual EGFR/VEGFR-2 Kinases Inhibitors: Design, Synthesis, Anticancer Evaluation and Docking Study," *RSC Advances* 14, no. 36 (2024): 26325–26339, https://doi.org/10.1039/d4ra04828h.

[43] S. K. Bishnoi, R. Shinde, and P. K. Sarkar, "12 Monkey Jack (Artocarpus Lakoocha Roxb.): Hope for Sustaining Livelihood" (2017).